

**OGLE-ing the Magellanic System:
Photometric Metallicity from Fundamental Mode RR Lyrae Stars**D. M. Skowron¹, I. Soszyński¹, A. Udalski¹, M. K. Szymański¹,
P. Pietrukowicz¹, J. Skowron¹, R. Poleski^{1,2}, Ł. Wyrzykowski¹,
K. Ulaczyk^{1,3}, S. Kozłowski¹, P. Mróz¹ and M. Pawlak¹¹ Warsaw University Observatory, Al. Ujazdowskie 4, 00-478 Warszawa, Poland² Department of Astronomy, Ohio State University, 140 W. 18th Ave., Columbus,
OH 43210, USA³ Department of Physics, University of Warwick, Gibbet Hill Road, Coventry,
CV4 7AL, UK

e-mail: dszczyg@astrouw.edu.pl

Received August 1, 2016

ABSTRACT

In an era of extensive photometric observations, the catalogs of RR Lyr type variable stars number tens of thousands of objects. The relation between the iron abundance [Fe/H] and the Fourier parameters of the stars light curve allows us to investigate mean metallicities and metallicity gradients in various stellar environments, independently of time-consuming spectroscopic observations. In this paper we use almost 6500 *V*- and *I*-band light curves of fundamental mode RR Lyr stars from the OGLE-IV survey to provide a relation between the *V*- and *I*-band phase parameter ϕ_{31} used to estimate [Fe/H]. The relation depends on metallicity, which limits its applicability. We apply this relation to metallicity formulae developed for the Johnson *V*- and the Kepler *Kp*-band to obtain the relation between [Fe/H] and ϕ_{31} for the *I*-band photometry. Last, we apply the new relation of Nemec to the OGLE-IV fundamental mode RR Lyr stars data and construct a metallicity map of the Magellanic Clouds. Median [Fe/H] is -1.39 ± 0.44 dex for the LMC and -1.77 ± 0.48 dex for the SMC, on the Jurcsik metallicity scale. We also find a metallicity gradient within the LMC with a slope of -0.029 ± 0.002 dex/kpc in the inner 5 kpc and -0.030 ± 0.003 dex/kpc beyond 8 kpc, and no gradient in-between (-0.019 ± 0.002 dex/kpc integrally). We do not observe a metallicity gradient in the SMC, although we show that the metal-rich RRab stars are more concentrated toward the SMC center than the metal-poor.

Key words: *Stars: abundances – Stars: statistics – Stars: variables: RR Lyr – Galaxies: abundances – Magellanic Clouds*

1. Introduction

The importance of RR Lyr (RRL) type variable stars in modern astrophysics cannot be underestimated: they serve as standard candles in our Galaxy and in the

Local Group, they trace the Galactic structure and evolution, they represent the old and metal-poor population that gives insight into the early chemical composition of the nearby Universe.

Physical parameters of the RRL pulsating variables are reflected in the characteristic shape of their light curves, that can be well modeled with the Fourier series. Several studies have shown that there exists a relation between the Fourier parameters and the iron abundance $[\text{Fe}/\text{H}]$ of RRL stars pulsating in the fundamental mode (RRab), and we will describe them in Section 2. Such a relation is of great importance in an era where photometric databases are orders of magnitude larger than spectroscopic ones, and we count RRL light curves in tens of thousands (Soszyński *et al.* 2014, 2016). This allows for studying the metal content of galaxies independently of spectroscopic observations which are much more time-consuming and difficult to collect, and in some cases even impossible to obtain. Large photometric databases of RRL stars have already been used to investigate the chemical characteristics of the Galactic bulge (Pietrukowicz *et al.* 2012, 2015, Gonzalez *et al.* 2013, Sans Fuentes and De Ridder 2014) and field (Kinemuchi *et al.* 2006, Szczygieł *et al.* 2009, Torrealba *et al.* 2015), and the Magellanic Clouds (Deb and Singh 2010, 2014, Deb *et al.* 2015, Feast *et al.* 2010, Haschke *et al.* 2012, Kapakos *et al.* 2011, 2012; Wagner-Kaiser and Sarajedini 2013).

In this paper, we take a look at available methods of determining $[\text{Fe}/\text{H}]$ from the light curve parameters, and by determining a transformation between the I - and the V -band phase parameters, we present a relation for an accurate $[\text{Fe}/\text{H}]$ calculation from the I -band RRab data. For this we use a sample of almost 6500 RRab stars from the fourth phase of the Optical Gravitational Lensing Experiment (OGLE-IV, Udalski, Szymański and Szymański 2015) with well observed light curves. We then apply the relation to the newest collection of RR Lyr type variables in the Magellanic Clouds (Soszyński *et al.* 2016) and construct a metallicity map of the Magellanic System.

It is worth noting, that the empirical relations presented in Section 2 should not be used for estimating $[\text{Fe}/\text{H}]$ for individual stars, but rather for statistically large datasets. For example, they can be used for determining mean iron abundances of globular clusters, metallicity gradients within galaxies, or for comparing metal content of different stellar structures.

2. Photometric Metallicity Calculation Methods for RRab stars

The first relation between the star's iron abundance and its light curve parameters was introduced by Kovács and Zsoldos (1995) and later improved by Jurcsik and Kovács (1996, hereafter JK96). In this method the metallicity is calculated from the stellar pulsation period P and the phase combination $\phi_{31} = \phi_3 - 3\phi_1$ from a sine series Fourier fit:

$$[\text{Fe}/\text{H}]_{JK} = -5.038 - 5.394P + 1.345\phi_{31}. \quad (1)$$

The formula was calibrated with 81 Galactic RRab stars that had accurate spectroscopic metallicities and well covered Johnson *V*-band light curves, and then tested on six Galactic and five Large Magellanic Cloud (LMC) globular clusters. The overall agreement of photometric and spectroscopic $[\text{Fe}/\text{H}]$ values was good, but there is a systematic difference at the low metallicity end ($[\text{Fe}/\text{H}] < -2.0$ dex) such that the photometric metallicities have higher values (by ≈ 0.3 dex).

Another method for calculating iron abundances from RRab light curves was proposed by Sandage (2004), where $[\text{Fe}/\text{H}]$ is calculated from the star's period and *V*-band light curve amplitude:

$$[\text{Fe}/\text{H}]_{\text{Sandage}} = -1.453A_V - 7.990 \log P - 2.145. \quad (2)$$

This formula is less sensitive to light curve quality, but as shown by Szczygieł *et al.* (2009), using 1227 All Sky Automated Survey (ASAS) RRab light curves, it has much larger scatter when compared to the JK96 method. The authors also show that it produces an unphysical bimodal distribution of photometric metallicities, which is a reflection of the Oosterhoff dichotomy, and is not seen with spectroscopically obtained $[\text{Fe}/\text{H}]$ values. Alcock *et al.* (2000) provide a similar relation, that uses the star's period and amplitude, thus it is also subject to larger $[\text{Fe}/\text{H}]$ scatter and the dependence on the Oosterhoff dichotomy.

The release of large catalogs of fine quality RRL light curves in the Cousins *I*-band by the OGLE group, encouraged Smolec (2005, hereafter S05) to estimate a new calibration of the $(P, \phi_{31}) \rightarrow [\text{Fe}/\text{H}]$ relation specifically for the *I*-band. It was based on 28 field RRab stars for which both spectroscopic and photometric data were available and is valid for Fourier sine series fit:

$$[\text{Fe}/\text{H}] = -3.142 - 4.902P + 0.824\phi_{31} \pm 0.646 \pm 0.375 \pm 0.104 \quad \sigma = 0.18 \quad (3)$$

This formula was calibrated in the metallicity range $-1.7 < [\text{Fe}/\text{H}] < 0.3$ dex.

Another attempt to determine $[\text{Fe}/\text{H}]$ from the *I*-band photometry was made by Deb and Singh (2010). The authors used good quality *V*- and *I*-band light curves of 29 stars in M3, to derive $V \leftrightarrow I$ interrelations between Fourier parameters ϕ_{21} , ϕ_{31} , and ϕ_{41} (from a cosine series fit), in order to be able to determine physical parameters of 352 RRL from OGLE-II *I*-band data for the Small Magellanic Cloud (SMC), which was much higher quality than the *V*-band data. In particular, they found a linear relation between ϕ_{31}^V and ϕ_{31}^I for RRab stars in the form:

$$\phi_{31}^V = 0.568\phi_{31}^I + 0.436 \pm 0.030 \pm 0.075 \quad (4)$$

and later used it together with the JK96 method to calculate photometric metallicities.

Deb and Singh (2014) compared metallicity values $[\text{Fe}/\text{H}]_S$ derived from the *I*-band light curves by S05 (Eq. 3), with metallicity values $[\text{Fe}/\text{H}]_{JK}$ (Eq. 1), after

converting ϕ_{31}^I to ϕ_{31}^V (Eq. 4). The comparison was done on a sample of 13 095 OGLE-III RRab light curves from the LMC and revealed that $[\text{Fe}/\text{H}]_S$ values are on average 0.07 dex higher than $[\text{Fe}/\text{H}]_{JK}$ values. The authors do not comment on this result, but possible explanations may include the small number of stars (29) used to derive Eq.(4), the small number of stars (28) used to derive Eq.(3), non-linearity of the $(\phi_{31}^I \rightarrow \phi_{31}^V)$ transformation, or additional dependence in that transformation.

A new $(P, \phi_{31}) \rightarrow [\text{Fe}/\text{H}]$ relation was derived by Nemeč *et al.* (2013) using 26 Kepler-field RRab stars with excellent light curves. The formula is nonlinear and agrees very well with spectroscopic iron abundances. Jeon, Ngeow and Nemeč (2014) provide the transformation from ϕ_{31}^V to ϕ_{31}^{Kp} , which together with the relation allows for calculating $[\text{Fe}/\text{H}]$ from the V -band light curve:

$$[\text{Fe}/\text{H}]_N = - 8.65 - 40.12P + 5.96\phi_{31}^{Kp} + 6.27\phi_{31}^{Kp}P - 0.72(\phi_{31}^{Kp})^2 \quad (5a)$$

$$\pm 4.64 \pm 5.18 \pm 1.72 \pm 0.96 \pm 0.17$$

$$\phi_{31}^{Kp} = \phi_{31}^V + 0.174 \quad (\pm 0.085) \quad (5b)$$

The above relation is the most up-to-date and should prove most accurate as it relies on very high quality and cadence light curves from the Kepler data for which high-resolution spectroscopic measurements were made with a derivation of $[\text{Fe}/\text{H}]_{spec}$ being a primary goal. It also corrects the problem of the JK96 formula overestimating $[\text{Fe}/\text{H}]$ by ≈ 0.3 dex at low metallicity values. This was partly due to smaller number of stars at low ($[\text{Fe}/\text{H}] < -2.0$ dex) metallicities and inaccurate spectroscopic metallicity adopted for *e.g.*, X Ari ($[\text{Fe}/\text{H}] = -2.10$ dex instead of $[\text{Fe}/\text{H}] \approx -2.65$ dex). However, the weak point of this method is Eq.(5b), which has a fairly large error of ± 0.085 and was based on only 34 stars, among which there were a few Blazhko RRab.

All the above relations are on the High Dispersion Spectroscopy (HDS) metallicity scale of Jurcsik (1995, hereafter J95).

In this paper, we want to calculate an accurate transformation between the phase parameter ϕ_{31} between the I - and the V -band. We think this is important for at least two reasons:

1. As one can see, most attempts to calculate the photometric metallicity rely either on the V -band light curves, or on a transformation of the phase parameter from I (or Kp) to V .
2. The only relation that directly uses the I -band data is the one of S05, but as noticed by Deb and Singh (2014), it shows an offset of 0.07 dex as compared to the formula of JK96, after transforming it to the I -band. However, the $(\phi_{31}^I \rightarrow \phi_{31}^V)$ transformation that was used had been determined with a small sample of only 29 stars, so its reliability may be questioned.

3. OGLE-IV Data

3.1. RRab Light Curves

For the purpose of this study we used the OGLE-IV RRab sample that consists of 27 258 stars in the Galactic bulge (Soszyński *et al.* 2014) and 27 081 in the LMC (Soszyński *et al.* 2016). We do not include the SMC RRL sample because of smaller number of observations in the V -band.

To ensure good Fourier fits to the light curves, we selected stars that have at least 80 observations in the V -band and at least 300 in the I -band. After this selection we were left with 14 755 objects: 14 033 in the LMC and 722 in the bulge. An average number of points per light curve is 640 in the I -band and 170 in the V -band.

3.2. Fourier Decomposition of the Light Curves

For each star we perform the Fourier analysis of its light curve, separately for the V - and the I -band in the form:

$$I(t) = A_0^V + \sum_{k=1}^n A_k^V \times \sin(2\pi kx + \phi_k^V)$$

$$V(t) = A_0^I + \sum_{k=1}^n A_k^I \times \sin(2\pi kx + \phi_k^I)$$

where $x = (\text{HJD} - \text{HJD}_0)/P$ and $n = 8$ is an order of the fit. We then shift all phases ϕ_k^V and ϕ_k^I to the $0-2\pi$ range.

Next we calculate phase combinations $\phi_{k1}^I = \phi_k^I - k\phi_1^I$ and $\phi_{k1}^V = \phi_k^V - k\phi_1^V$, where $k = 2, 3, 4, 5, 6$. According to the prescription of JK96 one should choose ϕ_{k1} such that it is closest to the mean observed sample average. They provide the observed averages for phase combinations in the V -band:

$$\langle \phi_{21}^V \rangle = 2.4, \langle \phi_{31}^V \rangle = 5.1, \langle \phi_{41}^V \rangle = 1.6, \langle \phi_{51}^V \rangle = 4.3, \langle \phi_{61}^V \rangle = 1.0$$

and draw attention to the careful choice of ϕ_{31}^V before using Eq.(1). Thanks to a large number of stars in our sample, we are able to determine precise sample averages in the $0-2\pi$ range in both bands, which mostly agree very well with those of JK96:

$$\langle \phi_{21}^V \rangle = 2.4, \langle \phi_{31}^V \rangle = 5.1, \langle \phi_{41}^V \rangle = 1.6, \langle \phi_{51}^V \rangle = 4.3, \langle \phi_{61}^V \rangle = 0.8,$$

$$\langle \phi_{21}^I \rangle = 2.8, \langle \phi_{31}^I \rangle = 5.8, \langle \phi_{41}^I \rangle = 2.6, \langle \phi_{51}^I \rangle = 5.6, \langle \phi_{61}^I \rangle = 2.2.$$

We then shift all ϕ_{k1}^V and ϕ_{k1}^I values within $\pm\pi$ of the sample averages.

3.3. The Sample Cleaning

The median scatter of observations around a Fourier model is 0.05 mag with a standard deviation of 0.02 mag in the I -band, and 0.05 mag with a standard deviation of 0.04 mag in the V -band. This scatter is mostly caused by Blazhko RRab stars, which constitute about 20% of all RRab stars in the LMC (Soszyński *et al.*

2009) and about 30% of all RRab in the Galactic bulge (Soszyński *et al.* 2011). According to recent Kepler and highest-quality ground based data, as many as 50% of RRab are expected to show the Blazhko effect (*e.g.*, Benkő *et al.* 2010). However, by applying the 50% cut to our data, we would risk removing non-modulated stars with higher light curve scatter, *e.g.*, faint stars that might be indistinguishable from Blazhko variables, and bias the sample. In order to clean our sample from Blazhko stars we reject objects based primarily on their *I*-band scatter, because there are 3–4 times as many observations in the *I*-band, making the detection of the true Blazhko effect much more secure. Thus we exclude RRab that have an *I*-band scatter larger than 0.07 mag, which removes $\approx 20\%$ of stars from our sample. We also exclude RRab variables that have a *V*-band scatter larger than 0.09 mag which leaves us with 11476 RRab. In order to further increase sample purity we also reject the faintest RRab stars with $I > 19$ mag and $V > 19.6$ mag which leaves 9527 RRab in the sample.

JK96 introduce a deviation parameter D_F for measuring the relative accuracy of the [Fe/H] prediction:

$$D_F = |F_{\text{obs}} - F_{\text{calc}}| / \sigma_F,$$

where F_{obs} is the observed value of a given Fourier parameter and F_{calc} is its predicted value based on other observed parameters and σ_F is the respective standard deviation. The relations used to calculate F_{calc} are provided in Table 6 of JK96. If the maximum deviation parameter for a given star $D_m = \max\{D_F\}$ is small ($D_m < 3$) then the light curve satisfies the compatibility condition and can be used for calculating the star's metallicity.

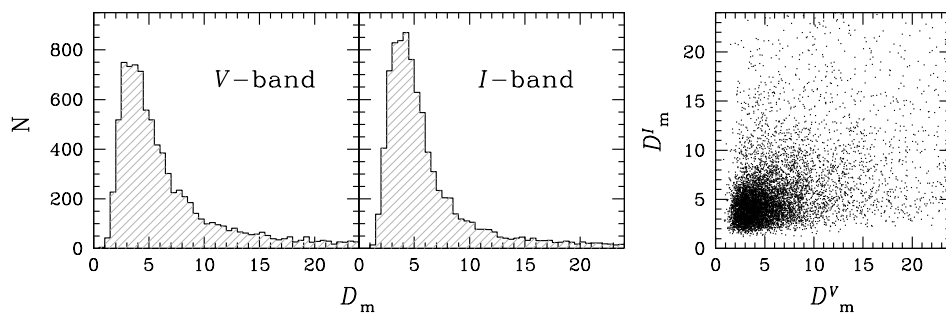


Fig. 1. Maximum deviation parameter distribution for a cleaned sample of 9527 RRab, calculated from the *V*-band data (*left panel*) and the *I*-band data (*middle panel*). *Right panel* shows the relation between the two deviation parameters.

Fig. 1 shows the distribution of D_m calculated from the *V*-band data (*left panel*) and the *I*-band data (*middle panel*). Only 16% of stars satisfy the condition $D_m < 3$ in the *V*-band, only 13% in the *I*-band, and barely 4% in both bands. It has been previously noticed (Szczygieł *et al.* 2009, Deb and Singh 2010) that the compatibility condition is indeed very strict and rejects many normal-looking light curves. Interestingly, there is also no correlation between D_m^V and D_m^I , as shown in the right

panel of Fig. 1, suggesting that $D_m < 3$ may not be the best criterion for "compatible light curve" selection. This seems probable, as the calibrating sample of JK96 used to derive parameter interrelations and the compatibility condition, had only 10 objects. Nevertheless, in order to avoid abnormal light curves, rather than select the ideal ones, we reject stars that have $D_m > 10$ in either band, that is 3089 (32%) stars in our sample, leaving us with 6438 RRab variables.

4. Photometric Metallicity Calculation

4.1. Relations between Phase Parameters ϕ_{k1}^V and ϕ_{k1}^I

In order to find the relations between phase parameters ϕ_{k1}^V and ϕ_{k1}^I , we first bin the data in steps of 0.05, 0.08, 0.1, 0.15, and 0.2 for $k = 2, 3, 4, 5$, and 6 respectively, both in the I - and V -band, requiring at least 40 points in the bin. Fig. 2 shows the data, where small gray dots mark all 6438 RRab and large gray dots represent the binned data. The dotted lines show the 1σ and 3σ range within the median. Next we fit a second order polynomial to the binned data in the form:

$$y = ax^2 + bx + c$$

where $x = \phi_{k1}^I$ and $y = \phi_{k1}^V$. The errors of the fit parameters (σ_a , σ_b , σ_c) are calculated using the bootstrap method for $N = 10000$ bootstrap samples. The final parameters of the fit are listed in Table 1 and in Fig. 2, where the red solid line represents the final fit.

The choice of the second order polynomial was preceded by a series of tests where other functions were fitted to the data. By comparing the χ^2 of the fits we were able to select the best-fitting function. Thanks to the large number of points we see that the relation is quadratic, rather than linear as found by Deb and Singh (2010), who had a sample of only 29 RRab stars. For comparison, their linear relation is plotted with a dashed line in the top right panel of Fig. 2.

Table 1

Fit parameters for $y = ax^2 + bx + c$

	a	b	c	σ_{fit}
$\phi_{21}^I \rightarrow \phi_{21}^V$	0.405 ± 0.033	-1.646 ± 0.179	3.815 ± 0.245	0.001
$\phi_{31}^I \rightarrow \phi_{31}^V$	0.122 ± 0.017	-0.750 ± 0.187	5.331 ± 0.523	0.004
$\phi_{41}^I \rightarrow \phi_{41}^V$	0.082 ± 0.013	0.247 ± 0.061	0.401 ± 0.070	0.009
$\phi_{51}^I \rightarrow \phi_{51}^V$	0.047 ± 0.010	0.141 ± 0.112	2.075 ± 0.307	0.019
$\phi_{61}^I \rightarrow \phi_{61}^V$	0.057 ± 0.011	0.364 ± 0.052	-0.357 ± 0.051	0.100

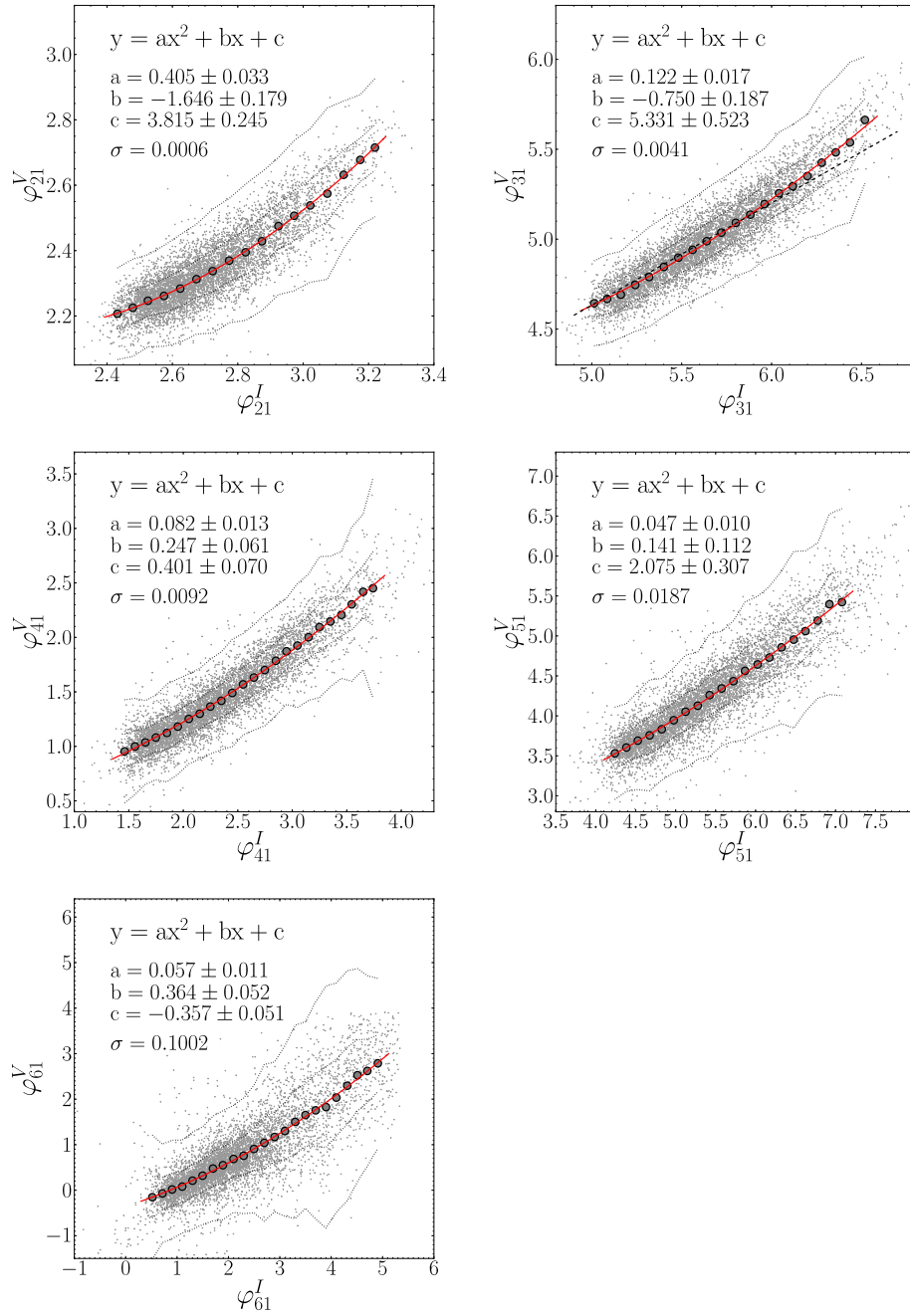


Fig. 2. Interrelations between phase parameters ϕ_{k1}^I and ϕ_{k1}^V . The red solid line is the second order polynomial fit to the large dots that represent the median value within a given bin. Fit parameters are given in Table 1 and in *all panels*. The dotted black lines mark 1σ and 3σ deviations from the median value. The dashed line in the *top right panel* shows the linear relation from Deb and Singh (2010). Note that the phase parameters come from a sine series fit to the light curves.

4.2. Photometric Metallicity Formula in the I-band

We use the interrelation ($\phi_{31}^I \rightarrow \phi_{31}^V$) estimated in Section 4.3:

$$\phi_{31}^V = 0.122(\phi_{31}^I)^2 - 0.750\phi_{31}^I + 5.331 \quad (6)$$

and paste it into the relation of JK96 (Eq. 1), thus obtaining the formula to calculate $[\text{Fe}/\text{H}]_{JK}$ based on the *I*-band light curve:

$$[\text{Fe}/\text{H}]_{JK}^I = 2.132 - 5.394P - 1.009\phi_{31}^I + 0.164(\phi_{31}^I)^2 \quad (7)$$

In order to see how accurate the calculation of the iron abundance is, in Fig. 3 we compare $[\text{Fe}/\text{H}]_{JK}$ (based on the *V*-band light curve, Eq. 1) with $[\text{Fe}/\text{H}]_{JK}^I$ (based on the *I*-band light curve, Eq. 7). We see that the differences can be very large, up to 0.4 dex, with a σ of 0.13 dex, which was expected when looking at the scatter in Fig. 2. This effect does not disappear if a more strict sample of the highest quality light curves is chosen (see the gray histogram in the left panel of Fig. 3. and black points in the right panel). Moreover, there is a clear correlation in the right panel of Fig. 3, which means that the ($\phi_{31}^I \rightarrow \phi_{31}^V$) interrelation may depend on metallicity.

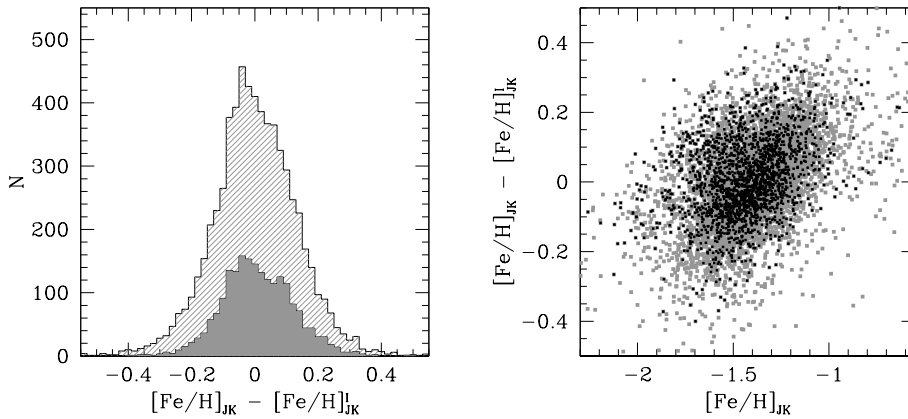


Fig. 3. *Left panel*: histogram of metallicity differences $[\text{Fe}/\text{H}]_{JK} - [\text{Fe}/\text{H}]_{JK}^I$. Dashed area represents all 6438 RRab, while the gray filled area a subset – 2034 RRab with highest quality light curves. *Right panel*: metallicity difference $[\text{Fe}/\text{H}]_{JK} - [\text{Fe}/\text{H}]_{JK}^I$ against $[\text{Fe}/\text{H}]_{JK}$ for the full sample (gray points) and for the high-quality sample (black points).

In order to verify if there is a metallicity dependence of the ($\phi_{31}^I \rightarrow \phi_{31}^V$) interrelation we repeat the fitting procedure described in Section 4.1, but this time for several metallicity bins. We first calculate the $[\text{Fe}/\text{H}]_{JK}$ photometric metallicity using the *V*-band light curve phase parameter. We then separate stars into eight metallicity bins chosen to ensure fair resolution and a sufficient number of stars in the bin, as presented in Table 2. The fitting results are shown in Fig. 4, where we plot ϕ_{31}^V vs. ϕ_{31}^I similarly as in Fig. 2, and each of the eight fits, represented with a different color line. We see a clear trend in ($\phi_{31}^I \rightarrow \phi_{31}^V$) dependence from the most

to the least metal poor RRab, especially for $\phi_{31}^I < 6$. Individual fit parameters are presented in Table 2.

Table 2
Metallicity bin characteristics and fit parameters

[Fe/H] _{JK} [dex]		N _{stars}	Fit parameters for $\phi_{31}^V = a(\phi_{31}^I)^2 + b\phi_{31}^I + c$			
range	median		a	b	c	σ_{fit}
≤ -1.7	-1.80	508	0.098 ± 0.065	-0.397 ± 0.733	4.043 ± 2.053	0.003
$(-1.7; -1.6]$	-1.64	526	0.049 ± 0.060	0.104 ± 0.682	2.792 ± 1.919	0.004
$(-1.6; -1.5]$	-1.55	979	0.161 ± 0.049	-1.164 ± 0.549	6.383 ± 1.530	0.003
$(-1.5; -1.4]$	-1.45	1251	0.023 ± 0.067	0.330 ± 0.754	2.356 ± 2.097	0.003
$(-1.4; -1.3]$	-1.35	1238	0.141 ± 0.041	-0.988 ± 0.459	6.072 ± 1.275	0.008
$(-1.3; -1.2]$	-1.26	962	0.091 ± 0.060	-0.440 ± 0.667	4.600 ± 1.853	0.006
$(-1.2; -1.1]$	-1.16	506	-0.079 ± 0.045	1.464 ± 0.504	-0.660 ± 1.416	0.001
> -1.1	-1.00	468	0.032 ± 0.040	0.218 ± 0.461	2.858 ± 1.337	0.002

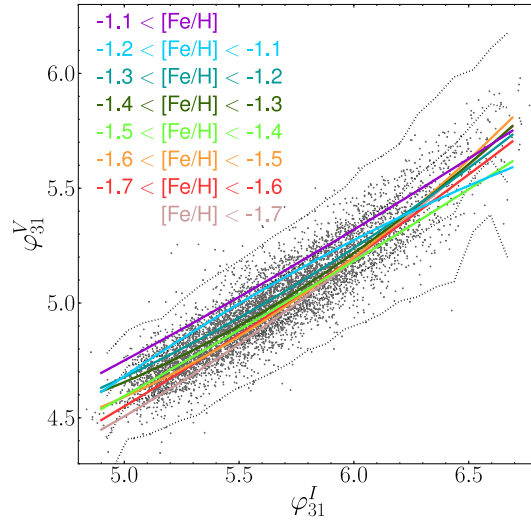


Fig. 4. Interrelation between phase parameters ϕ_{31}^I and ϕ_{31}^V . Dots represent the same sample of RRab as in Fig. 2 and the dotted black lines mark 1σ and 3σ deviations from the median value. Different color lines mark second order polynomial fits within different JK96 metallicity bins, as described in the legend. Fit parameters are given in Table 2.

We then calculate $[\text{Fe}/\text{H}]_{N1}^I$ for each star using the relation of N13 (Eq. 5) and the $(\phi_{31}^I \rightarrow \phi_{31}^V)$ transformation from Eq.(6). The resulting formula becomes quite complicated with eight elements and ϕ_{31}^I to the fourth power, so we will refrain from providing it in that form, also because repeated rounding of the coefficients lowers the final accuracy. We also calculate $[\text{Fe}/\text{H}]_{N2}^I$ using the relation of N13 (Eq. 5) and the $(\phi_{31}^I \rightarrow \phi_{31}^V)$ transformation, but this time the transformation equation coefficients are taken from Table 2, *i.e.*, they depend on the stars

metallicity. The results are presented in Fig. 5. The left panel shows how metallicities calculated from metallicity dependent and independent formulae change with metallicity, which was expected from Figs. 3 and 4. The histogram of these differences ($[\text{Fe}/\text{H}]_{N1}^I - [\text{Fe}/\text{H}]_{N2}^I$) is presented in the middle panel of Fig. 5. The $[\text{Fe}/\text{H}]_{N1}^I - [\text{Fe}/\text{H}]_{N2}^I$ differences for individual stars reach 0.3 dex, but are typically lower than 0.1 dex. Finally, the right panel shows a histogram of photometric metallicities $[\text{Fe}/\text{H}]_{N1}^I$ and $[\text{Fe}/\text{H}]_{N2}^I$. Both distributions have a similar shape, although the metallicity dependent formula produces a slightly wider profile. Nevertheless, the overall similarity of the two distributions is reassuring – even though we are not able to obtain a single relation between ϕ_{31}^I and ϕ_{31}^V because it depends on metallicity, the difference between results, *i.e.*, whether accounting for that dependence or not, is not very large. As stressed before, this is true only when statistically analyzing large samples of RRab, not in the case of star-to-star comparisons.

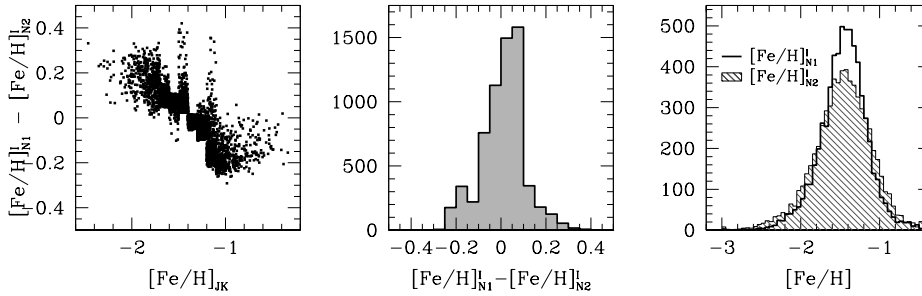


Fig. 5. Comparison of photometric metallicities calculated using metallicity independent ($[\text{Fe}/\text{H}]_{N1}^I$) and metallicity dependent ($[\text{Fe}/\text{H}]_{N2}^I$) formulae. *Left panel:* metallicity difference $[\text{Fe}/\text{H}]_{N1}^I - [\text{Fe}/\text{H}]_{N2}^I$ vs. $[\text{Fe}/\text{H}]_{JK}$. *Middle panel:* a histogram of metallicity differences $[\text{Fe}/\text{H}]_{N1}^I - [\text{Fe}/\text{H}]_{N2}^I$. *Right panel:* a histogram of $[\text{Fe}/\text{H}]_{N1}^I$ and $[\text{Fe}/\text{H}]_{N2}^I$.

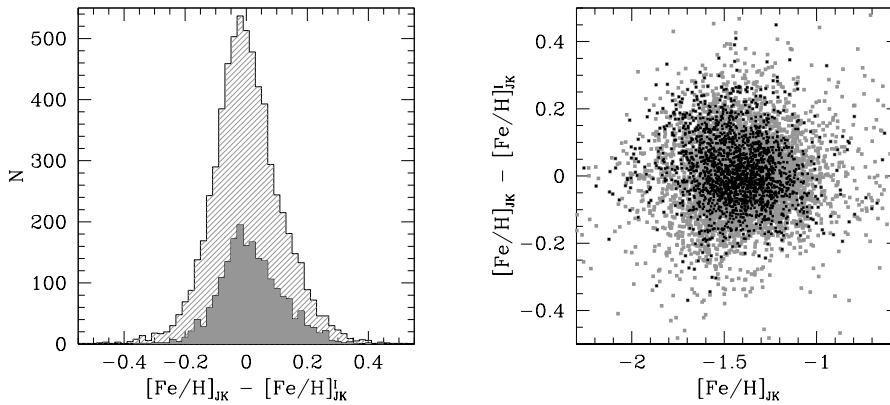


Fig. 6. Analog of Fig. 3, only this time the metallicity dependence of the ($\phi_{31}^I \rightarrow \phi_{31}^V$) interrelation is taken into account. *Left panel:* histogram of metallicity differences $[\text{Fe}/\text{H}]_{JK} - [\text{Fe}/\text{H}]_{JK}^I$. Dashed area represents all 6438 RRab, while the gray filled area a subset – 2034 RRab with highest quality light curves. *Right panel:* metallicity difference $[\text{Fe}/\text{H}]_{JK} - [\text{Fe}/\text{H}]_{JK}^I$ against $[\text{Fe}/\text{H}]_{JK}$ for the full sample (gray points) and for the high-quality sample (black points).

Fig. 6 is an analog of Fig. 3, *i.e.*, it compares $[\text{Fe}/\text{H}]_{JK}$ (based on the V -band light curve, Eq. 1) with $[\text{Fe}/\text{H}]_{JK}^I$ (based on the I -band light curve). Only this time we are not using a single Eq.(6) to transform ϕ_{31}^I to ϕ_{31}^V , but a set of equations from Table 2, which are then pasted into Eq.(1). We see, that after accounting for the metallicity dependence of the ($\phi_{31}^I \rightarrow \phi_{31}^V$) interrelation, the correlation visible in Fig. 3 vanishes in Fig. 6, although the scatter remains high, suggesting that this is an intrinsic property of this interrelation.

4.3. Applicability of the ($\phi_{31}^I \rightarrow \phi_{31}^V$) interrelation

As shown in this section, the applicability of the ($\phi_{31}^I \rightarrow \phi_{31}^V$) transformation is limited. Since it depends on metallicity, there is a set of equations instead of one, and deciding which of those equations should be used, requires knowing the $[\text{Fe}/\text{H}]_{JK}$ metallicity a priori. However, the fact that one needs to use the ($\phi_{31}^I \rightarrow \phi_{31}^V$) transformation means that the $[\text{Fe}/\text{H}]_{JK}$ calculation is not possible, as there is no V -band data available. In such case, one idea is to iterate the whole process, until the most accurate photometric metallicity is calculated. Another, simpler, idea is to use the mean relation between ϕ_{31}^I and ϕ_{31}^V , *i.e.*, Eq.(6). As shown in Fig. 5, such distribution will be still overestimated at lowest $[\text{Fe}/\text{H}]$ and underestimated at highest $[\text{Fe}/\text{H}]$ (see left panel), but for the majority of stars the differences will be < 0.1 dex (see middle panel). In the case of a large sample this effect does not change the overall distribution significantly – median and standard deviations of the two histograms in the right panel of Fig. 5 are: $\langle [\text{Fe}/\text{H}]_{N1}^I \rangle = -1.44 \pm 0.31$ dex, and $\langle [\text{Fe}/\text{H}]_{N2}^I \rangle = -1.45 \pm 0.38$ dex.

4.4. Comparison of $[\text{Fe}/\text{H}]$ from Three Methods

We calculate photometric metallicities for 6438 RRab using three methods: $[\text{Fe}/\text{H}]_S$ (Eq. 3), $[\text{Fe}/\text{H}]_{JK}^I$ (Eq. 1 after transforming ϕ_{31}^I to ϕ_{31}^V), and $[\text{Fe}/\text{H}]_{N2}^I$ (Eq. 5 after transforming ϕ_{31}^I to ϕ_{31}^V). The transformations in the latter two were calculated based on parameters from Table 2. The left panel of Fig. 7 compares the results and shows metallicity distributions for the three formulae. Median and standard deviation values are as follows: $\langle [\text{Fe}/\text{H}]_S \rangle = -1.29 \pm 0.19$ dex, $\langle [\text{Fe}/\text{H}]_{JK}^I \rangle = -1.40 \pm 0.25$ dex, and $\langle [\text{Fe}/\text{H}]_{N2}^I \rangle = -1.45 \pm 0.38$ dex. All presented distributions are different – the S05 method produces highest metallicity values with the lowest dispersion, the transformed JK96 method gives lower metallicity values and the higher dispersion. $[\text{Fe}/\text{H}]_{N2}^I$ is not only shifted toward lower metallicities, but also has a much flatter and wider profile. We checked that this is not an effect of error propagation during ($\phi_{31}^I \rightarrow \phi_{31}^V$) and ($\phi_{31}^V \rightarrow \phi_{31}^{Kp}$) transformations and it is actually expected after compensating for $[\text{Fe}/\text{H}]_{JK}^I$ overestimation at low metallicity values. The difference between $[\text{Fe}/\text{H}]_{JK}^I$ and $[\text{Fe}/\text{H}]_{N2}^I$ is further pictured in the right panel of Fig. 7. The overall agreement between the two methods is rather poor, especially at the low metallicity end. The same is true, when instead of $[\text{Fe}/\text{H}]_{N2}^I$ we use $[\text{Fe}/\text{H}]_{N1}^I$, *i.e.*, the metallicity independent formula – the distribu-

tion of $[\text{Fe}/\text{H}]_{N1}^I$ is only slightly different from that of $[\text{Fe}/\text{H}]_{N2}^I$, as already shown in the right panel of Fig. 5, and so does not change the conclusions.

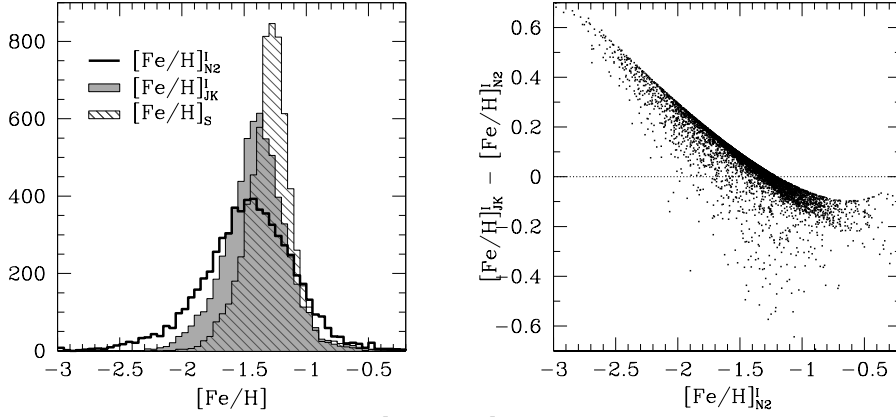


Fig. 7. *Left panel:* histograms of $[\text{Fe}/\text{H}]_{N2}^I$, $[\text{Fe}/\text{H}]_{JK}^I$, and $[\text{Fe}/\text{H}]_S$ for the 6438 RRab. *Right panel:* metallicity difference $[\text{Fe}/\text{H}]_{JK}^I - [\text{Fe}/\text{H}]_{N2}^I$ vs. $[\text{Fe}/\text{H}]_{N2}^I$.

Deb *et al.* (2015) in their analysis of the SMC RRab sample from OGLE-III decided to use the relation of JK96 to calculate iron abundances, rather than that of N13, because they had found that formal errors on $[\text{Fe}/\text{H}]_N$ (Eq. 5a) are much larger than those on $[\text{Fe}/\text{H}]_{JK}$. However, this means overestimating $[\text{Fe}/\text{H}]$ at low metallicities. We think that larger errors on individual $[\text{Fe}/\text{H}]$ values are not as problematic when doing a statistical analysis of a large sample, as an overestimation of the sample's global properties such as median iron abundances and their gradients. Thus we decide to use the relation of N13. The formal errors on $[\text{Fe}/\text{H}]_N$ (Eq. 5a) are indeed nonphysically large, so we will do not list them in this paper. Instead, we calculate errors for each star individually, as described in Section 6.

5. Photometric Metallicity in the Magellanic System

We use the full dataset of 32 581 RRab stars from Soszyński *et al.* (2016) to create a photometric metallicity map of the Magellanic System. First, we clean the sample by excluding objects with no V -band magnitude and with large errors of phase parameters used for $[\text{Fe}/\text{H}]$ estimation. We also remove Blazhko stars, which we identify by the scatter of the light curve around the Fourier model, and remove about 20% of stars with the largest scatter. This leaves 24 133 objects in the final sample, among which 20 573 belong to the LMC and 3560 to the SMC.

5.1. Metallicity Distribution

We then calculate photometric metallicities using the most accurate to date relation of N13 (Eq. 5) after transforming it to the I -band with Eq.(6). We decided to use a single relation for the $(\phi_{31}^I \rightarrow \phi_{31}^V)$ transformation rather than a set of equations from Table 2, because the V -band data for many RRab are poor (see discussion

in Section 4.3). The formal errors of the N13 relation, using the standard error propagation formula, become unrealistically large, resulting in extremely high values of $\sigma_{[\text{Fe}/\text{H}]}$. In such case we decided to perform an error simulation. For each star, we randomly select all coefficients in each equation, from their own distributions (assuming they are Gaussian), and calculate $[\text{Fe}/\text{H}]_i$. This is repeated 1000 times for each star. The standard deviation of the resulting distribution is then treated as the error of $[\text{Fe}/\text{H}]$.

The distribution of metallicities is presented in Fig. 8 for both the LMC (left panel) and the SMC (right panel). Median metallicity values are $[\text{Fe}/\text{H}]_{\text{J95}} = -1.39 \pm 0.44$ dex on the HDS scale of J95, and $[\text{Fe}/\text{H}]_{\text{ZW84}} = -1.59 \pm 0.31$ dex on the Zinn and West (1984, hereafter ZW84) scale. In the case of the SMC, median iron abundances are $[\text{Fe}/\text{H}]_{\text{J95}} = -1.77 \pm 0.48$ dex and $[\text{Fe}/\text{H}]_{\text{ZW84}} = -1.85 \pm 0.33$ dex. We used the equation of J95 in the form: $[\text{Fe}/\text{H}]_{\text{ZW84}} = ([\text{Fe}/\text{H}]_{\text{J95}} - 0.88)/1.431$ to transform from the HDS scale of J95 to the ZW84 scale. Some studies use the relation of Papadakis *et al.* (2000) for this purpose ($[\text{Fe}/\text{H}]_{\text{ZW84}} = 1.028[\text{Fe}/\text{H}]_{\text{J95}} - 0.242$), which gives similar results as the relation of J95 around $[\text{Fe}/\text{H}] \simeq -1.4$ dex, but quickly offsets, *e.g.*, at $[\text{Fe}/\text{H}] \simeq -2.0$ dex the difference between the two transformations is -0.23 dex and at $[\text{Fe}/\text{H}] \simeq 0.0$ dex it is 0.53 dex. Papadakis *et al.* (2000) do not explain in detail how their relation was obtained, so it is not clear how reliable the relation is and what systematic errors it may be subject to. For this reason we use the relation of J95 throughout the paper.

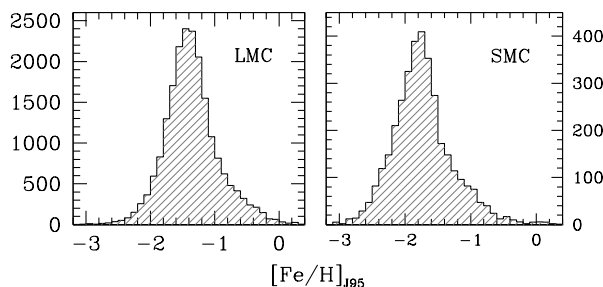


Fig. 8. Histograms of $[\text{Fe}/\text{H}]_N^I$ on the J95 metallicity scale.

Distances are calculated from the reddening-free Wesenheit index in order to avoid correcting for extinction. The observed Wesenheit magnitude is:

$$W = I - 1.55 \times (V - I)$$

and the absolute Wesenheit magnitude is:

$$W_0 = -1.039 - 2.524 \log P + 0.147([\text{Fe}/\text{H}]_{N,C}^I + 0.04)$$

from Table 5 of Braga *et al.* (2015). $[\text{Fe}/\text{H}]_{N,C}^I$ is the iron abundance on the Carretta *et al.* (2009) metallicity scale, which was obtained by transforming $[\text{Fe}/\text{H}]_N^I$ from the HDS scale of J95 to the Carretta scale with: $[\text{Fe}/\text{H}]_{\text{C09}} = 1.001[\text{Fe}/\text{H}]_{\text{J95}} -$

0.112 (Kapakos *et al.* 2011). Median LMC distance is $D_{\text{LMC}} = 50.56$ kpc, while median SMC distance is $D_{\text{SMC}} = 60.45$ kpc. We also calculate the three-dimensional coordinates for each object using transformation equations from van der Marel and Cioni (2001) and Weinberg and Nikolaev (2001):

$$x = -d \times \cos(\delta) \sin(\alpha - \alpha_{\text{cen}}) \quad (8)$$

$$y = d \times (\sin(\delta) \cos(\delta_{\text{cen}}) - \cos(\delta) \sin(\delta_{\text{cen}}) \cos(\alpha - \alpha_{\text{cen}})) \quad (9)$$

$$z = d \times (\cos(\delta) \cos(\delta_{\text{cen}}) \cos(\alpha - \alpha_{\text{cen}}) + \sin(\delta) \sin(\delta_{\text{cen}})) - D_{\text{cen}} \quad (10)$$

where d is the objects distance from observer, α_{cen} and δ_{cen} are the LMC/SMC center equatorial coordinates and D_{cen} is the median LMC/SMC distance. We adopt $\alpha_{\text{LMC}} = 80.38$ deg, $\delta_{\text{LMC}} = -69.61$ deg, and $\alpha_{\text{SMC}} = 13.95$ deg, $\delta_{\text{SMC}} = -72.78$ deg, which are the centers of the distributions of α and δ in both galaxies. Having (x, y, z) for each RRab we then calculate their distances from the LMC/SMC center as $r = \sqrt{x^2 + y^2 + z^2}$. The three-dimensional distribution of OGLE-IV RR Lyr will be discussed in detail in Jacyszyn-Dobrzyniecka *et al.* (in preparation).

Finally, in Fig. 9 we plot two-dimensional metallicity maps of the Magellanic System. The top map shows all individual $[\text{Fe}/\text{H}]$ values, with the point size getting smaller toward galaxy centers, to increase the visible resolution. In the bottom map, we plot averaged iron abundances in regions where the number of stars in an area bin (≈ 0.335 deg²) was at least five, and leave individual measurements otherwise. By comparing two maps we see that there is a large spread in $[\text{Fe}/\text{H}]$ in every direction in the Clouds, but after averaging, all areas seem to have a nearly constant median $[\text{Fe}/\text{H}]$ value. While the SMC does not seem to have a metallicity gradient, we do see that the LMC has a higher average metallicity in the center as compared to the outer regions.

Metallicities and locations of all 24 133 RRab in our sample are available in an electronic form from the OGLE website:

<http://ogle.astrouw.edu.pl>

The first few lines of the file are presented in Table 3.

T a b l e 3

Metallicities of 24 133 OGLE-IV RRab stars

ID	α [deg]	δ [deg]	D [kpc]	$[\text{Fe}/\text{H}]_{J95}$	$[\text{Fe}/\text{H}]_{ZW84}$
lmc502_08_6887	81.655250	-70.702472	51.65	-1.510 ± 0.087	-1.670 ± 0.061
lmc563_28_7986	88.958750	-65.657083	46.75	-1.470 ± 0.039	-1.642 ± 0.027
lmc556_21_903	85.632917	-65.586028	48.58	-0.601 ± 0.451	-1.035 ± 0.315
lmc551_14_16904	86.225667	-71.925306	49.26	-2.419 ± 0.087	-2.306 ± 0.061
...

Full table is available for download from the OGLE website: <http://ogle.astrouw.edu.pl>

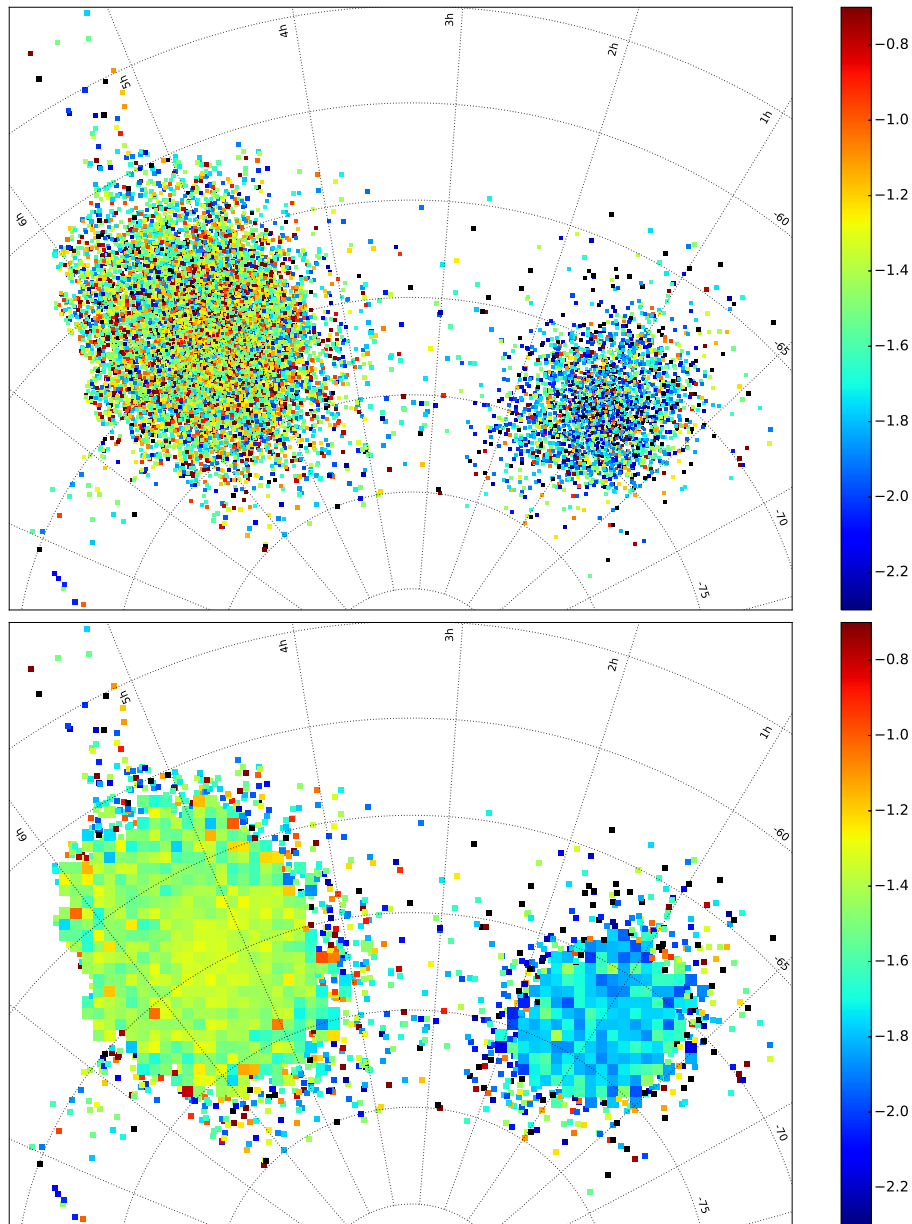


Fig. 9. Metallicity maps of the Magellanic System on the J95 metallicity scale. *Top*: all individual $[\text{Fe}/\text{H}]$ measurements, *bottom*: binned $[\text{Fe}/\text{H}]$ in the galaxy centers and individual in the outskirts, where number of stars per area bin ($\approx 0.335 \text{ deg}^2$) was less than five.

5.2. Metallicity Gradient

In order to better see whether there is a metallicity gradient in the galaxies, in Fig. 10 we plot $[\text{Fe}/\text{H}]$ vs. radial distance r from the LMC/SMC center. Gray dots show all 24 133 RRab variables used in the analysis, 20 573 in the LMC (left) and 3560 in the SMC (right). Large gray circles mark median metallicity values in

1 kpc wide bins, requiring at least 40 points in the bin in the case of the LMC and 20 in the case of the SMC. Dotted lines mark 1σ and 3σ deviations from the median value in a given bin. While there appears to be no metallicity gradient in the SMC, we clearly see that in the LMC $[\text{Fe}/\text{H}]$ decreases with distance from the center. The decline is evident within 4 kpc from the galaxy center, then the metallicity remains constant until about 8 kpc, when it shows another mild decline. The slope of the gradient is -0.029 ± 0.002 dex/kpc in the inner 5 kpc and -0.030 ± 0.003 dex/kpc beyond 8 kpc. For the entire galaxy, the slope is -0.019 ± 0.002 dex/kpc.

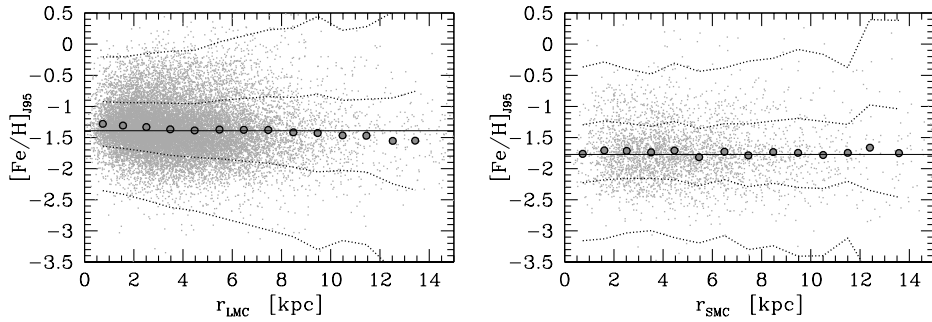


Fig. 10. Metallicity vs. distance from the galaxy center for the LMC (*left*) and the SMC (*right*). Gray dots show all 24 133 RRab used in the analysis. Large gray circles mark median metallicity values in 1 kpc wide bins, requiring at least 40 points in the bin in the case of the LMC and 20 in the case of the SMC. Solid line shows the median iron abundance of -1.39 dex in the LMC and -1.77 dex in the SMC. Dotted lines mark 1σ and 3σ deviations from the median value.

The significance of the result could be argued due to the large scatter (and errors) in $[\text{Fe}/\text{H}]$, but Fig. 11 further supports the finding. The plot shows how the ratio of a number of stars with high metallicities N_{HIGH} to a number of stars with low metallicities N_{LOW} , changes with the distance from the center of each galaxy $r_{\text{LMC/SMC}}$. In other words, N_{HIGH} is the number of stars for which $[\text{Fe}/\text{H}] > F_1$ while N_{LOW} is the number of stars for which $[\text{Fe}/\text{H}] < F_2$ in a given distance bin. In the case of the LMC $F_1 = -0.55$ dex and $F_2 = -2.0$ dex, while for the

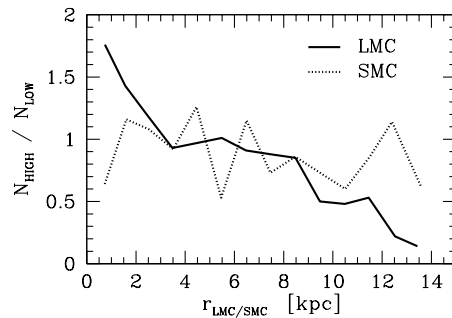


Fig. 11. Ratio of a number of stars vs. distance from the galaxy center for the LMC (solid line) and the SMC (dotted line). N_{HIGH} is the number of stars for which $[\text{Fe}/\text{H}] > F_1$ while N_{LOW} is the number of stars for which $[\text{Fe}/\text{H}] < F_2$. In the case of the LMC $F_1 = -0.55$ dex and $F_2 = -2.0$ dex, while for the SMC $F_1 = -1.3$ dex and $F_2 = -2.15$ dex.

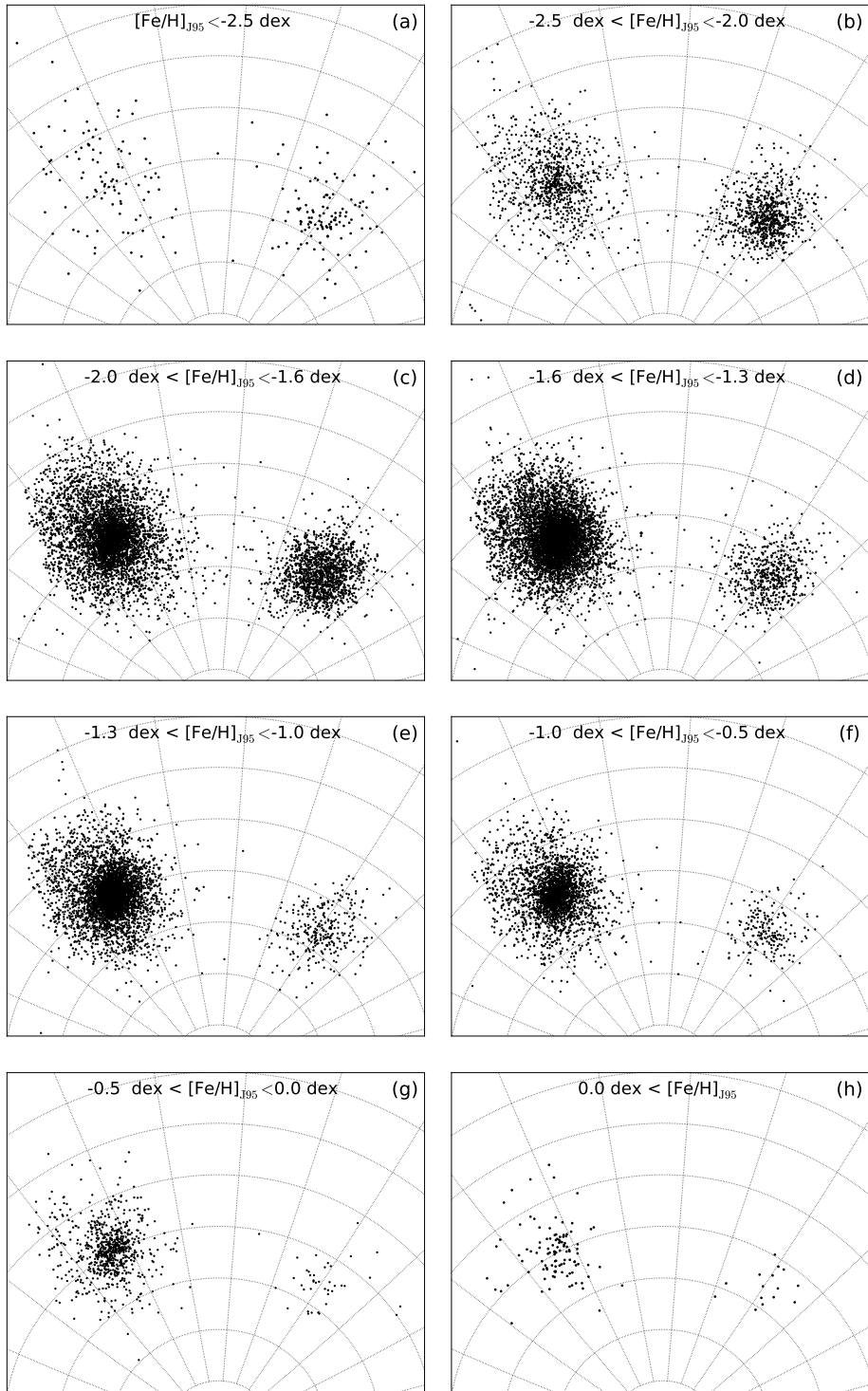


Fig. 12. Metallicity tomography of the Magellanic System, starting from low metallicities (*panel a*) to high metallicities (*panel h*).

SMC $F_1 = -1.3$ dex and $F_2 = -2.15$ dex. F_1 and F_2 were chosen such that the ratio $N_{\text{HIGH}}/N_{\text{LOW}} = 1$ for the entire galaxy and that the number of stars N_{HIGH} and N_{LOW} in each distance bin was reasonable. Fig. 11 shows that the center of the LMC has more metal-rich RRab than the outskirts of this galaxy, suggesting an existence of the metallicity gradient. As noted before, $[\text{Fe}/\text{H}]$ declines within ≈ 4 kpc from the center, then plateaus until about 8 kpc when the second decline begins. On the other hand, no significant metallicity change is observed in the SMC, as concluded from Fig. 10.

Last, in Fig. 12 we show the two dimensional distribution of RRab stars from eight metallicity bins, starting from low metallicity $[\text{Fe}/\text{H}] < -2.5$ dex, panel (a), and ending at high metallicity $[\text{Fe}/\text{H}] > 0$ dex, panel (h). Note that the metallicity range within a bin varies from 0.5 dex to 0.3 dex, in order to compensate for higher stellar density around $[\text{Fe}/\text{H}]$ distribution maxima. In the case of the LMC, metal-rich RRab stars prefer the centers of the galaxies, while the metal-poor are evenly distributed. In the case of the SMC, this is not as well pronounced, but we do see that the most metal-rich RRab (panel h) are more concentrated than most metal-poor RRab (panel a). The Magellanic Bridge RRab pulsators tend to have lower metallicities (panels a to d), with a slighter preference of lower metallicities typical for the SMC ($-2.0 < [\text{Fe}/\text{H}] < -1.6$ dex, panel (c)). We do not observe high metallicity RRab stars in the Magellanic Bridge (panels g and h).

5.3. *Is the Metallicity Gradient Real?*

Photometric metallicities in the Magellanic System, presented in this section, were calculated using the method of N13 and the metallicity independent transformation between ϕ_{31}^I and ϕ_{31}^V . As discussed in Section 4.3, choosing a metallicity independent over the metallicity dependent ($\phi_{31}^I \rightarrow \phi_{31}^V$) interrelation, results in overestimating $[\text{Fe}/\text{H}]$ at the low end of the distribution and underestimating it at the high end. While the mean metallicity values for the LMC and the SMC are not affected, the metallicity gradient may be sensitive to such systematic changes. This poses the question about the reality and validity of our results.

In order to check how the choice of the photometric metallicity calculation method affects the metallicity distribution, we repeat calculations from Sections 5.1 and 5.2, but this time using the relation of S05 (Eq. 3), which was calibrated on the *I*-band light curves and thus does not need any additional transformations. Median and standard deviation values of the resulting distributions are $\langle [\text{Fe}/\text{H}]_S \rangle = -1.27 \pm 0.25$ dex for the LMC and $\langle [\text{Fe}/\text{H}]_S \rangle = -1.48 \pm 0.26$ dex for the SMC. As already shown in the left panel of Fig. 7 and discussed in Section 4.4, the S05 method produces the highest mean $[\text{Fe}/\text{H}]$ of all methods, with the lowest dispersion, and significantly overestimates $[\text{Fe}/\text{H}]$ at the low metallicity end, as compared to $[\text{Fe}/\text{H}]_{JK}$ and $[\text{Fe}/\text{H}]_N$.

The $[\text{Fe}/\text{H}]_S$ metallicity distribution in the Magellanic Clouds is very similar to that presented in Fig. 9, only its high and low end limits are different, so we do

not include an additional figure to illustrate this. What is interesting, is whether there is a change in $[\text{Fe}/\text{H}]$ with the distance from the centers of the two galaxies. In Fig. 13 we show the metallicity gradient both in the LMC and the SMC. The general conclusion is very similar to that from Fig. 11 – we observe a metallicity gradient in the LMC, while there seems to be no gradient in the SMC. The difference is that Fig. 13 does not have the plateau seen in Fig. 11, and the slope of the gradient is lower: -0.011 ± 0.001 dex/kpc as opposed to -0.019 ± 0.002 dex/kpc (total). Such differences are expected since the two distributions are different. The presence of the metallicity gradient in the LMC, independently of the method used, confirms its reality.

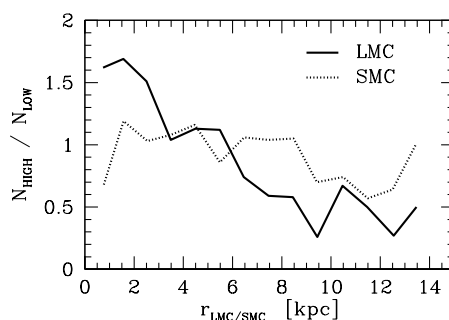


Fig. 13. Similar as Fig. 11, but for the $[\text{Fe}/\text{H}]_S$ photometric metallicity. Ratio of a number of stars vs. distance from the galaxy center for the LMC (solid line) and the SMC (dotted line). N_{HIGH} is the number of stars for which $[\text{Fe}/\text{H}] > F_1$ while N_{LOW} is the number of stars for which $[\text{Fe}/\text{H}] < F_2$. In the case of the LMC $F_1 = -0.8$ dex and $F_2 = -1.65$ dex, while for the SMC $F_1 = -1.37$ dex and $F_2 = -1.6$ dex.

6. Comparison with Previous Photometric Metallicity Studies of the Magellanic Clouds

6.1. Metallicity Distribution

There have been numerous studies of photometric metallicity in the Magellanic Clouds using RR Lyr type stars. Methods for $[\text{Fe}/\text{H}]$ calculation used by various authors were either those using period and amplitude (by Alcock *et al.* 2000 and Sandage 2004) or those using a linear relation between period and ϕ_{31} (by JK96 and S05). Since this is the first work that applies the relation of N13 to construct the photometric metallicity map of the Magellanic System, we may expect to see lower on average metallicities than in other publications, as the new relation provides lower metallicity values at the low end of the $[\text{Fe}/\text{H}]$ distribution.

Mean metallicity values from the literature are listed in Table 4, in the J95 and ZW84 metallicity scale, depending upon availability. In the case of the LMC, all the cited studies provide $[\text{Fe}/\text{H}]$ in the ZW84 scale and only one in the scale of J95, while in the case of the SMC it is the opposite. Table 4 also provides information

Table 4

Photometric metallicity in the Magellanic Clouds from RRab stars

REFERENCE	EQN.*	DATA	LMC		SMC	
			J95	ZW84	J95	ZW84
Deb and Singh (2010)	JK96	O-II	–	–	-1.56 ± 0.25	–
Kapakos <i>et al.</i> (2011)	JK96	O-III	–	–	-1.51 ± 0.41	–
Kapakos <i>et al.</i> (2012)	JK96	O-III	–	–	-1.58 ± 0.41	–
Haschke <i>et al.</i> (2012)	S05	O-III	-1.22 ± 0.26	-1.49 ± 0.26	-1.42 ± 0.33	-1.70 ± 0.33
Wagner-Kaiser and Sarajedini (2013)	A00	O-III	–	-1.70 ± 0.25	–	–
	S05	O-III	–	-1.63 ± 0.21	–	–
Deb and Singh (2014)	JK96	O-III	–	-1.57 ± 0.12	–	–
	S05	O-III	–	-1.50 ± 0.12	–	–
	A00	O-III	–	-1.67 ± 0.18	–	–
	Sd04	O-III	–	-1.57 ± 0.20	–	–
This work	N13	O-IV	-1.39 ± 0.44	-1.59 ± 0.31	-1.77 ± 0.48	-1.85 ± 0.33

*Methods of metallicity calculation: A00 – Alcock *et al.* (2000), JK96 – Jurcsik and Kovacs (1996), S05 – Smolec (2005), Sd04 – Sandage (2004), N13 – Nemec *et al.* (2013)

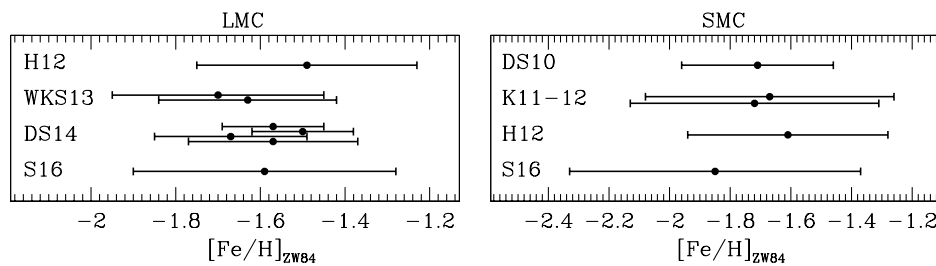


Fig. 14. Different $[Fe/H]$ estimations for the LMC (*left*) and the SMC (*right*) from the literature and this work, as listed in Table 4. Symbols are as follows: DS10 – Deb and Singh (2010), DS14 – Deb and Singh (2014), H12 – Haschke *et al.* (2012), K11 – Kapakos *et al.* (2011), K12 – Kapakos and Hatzidimitriou (2012), WKS13 – Wagner-Kaiser and Sarajedini (2013), S16 – this work. Note that all points are on the ZW84 metallicity scale – SMC points from Table 4 have been transformed from the J95 metallicity scale with the same equation (by J95).

about the method and data used to calculate the iron abundances. Note that all studies are based on the OGLE data.

The numbers from Table 4 are visualized in Fig. 14 – for the LMC in the left panel and for the SMC in the right panel, both on the ZW84 scale. All SMC $[Fe/H]$ values from Table 4 have been transformed from the J95 to the ZW84 metallicity scale with the same equation (by J95), including the value of Haschke *et al.* (2012), which was originally calculated using the equation of Papadakis *et al.* (2000), and that original value is provided in Table 4. We do not recalculate $[Fe/H]_{ZW84}$ for the LMC, because the difference between the transformations of J95 and Papadakis *et al.* (2000) is very small.

In the case of the LMC all $[Fe/H]$ estimates from different methods are well consistent and the mean value is $[Fe/H]_{ZW84} = -1.59$ dex, which corresponds to

$[\text{Fe}/\text{H}]_{J95} = -1.39$ dex. This is because the metallicity of the LMC is in the “safe” range, where all methods give roughly similar results. In the case of the more metal-poor SMC, there is a noticeable discrepancy between values from the literature and the result of this study, which is expected as a consequence of Fig. 7: median metallicity from Haschke *et al.* (2012) with S05 method is the highest, while the result of this study with N13 method is the lowest.

6.2. Metallicity Gradient

The metallicity gradient in the LMC has been found in asymptotic giant branch (AGB) stars (derived by Cioni 2009) and from OGLE-III RRab stars (Feast *et al.* 2010, Wagner-Kaiser and Sarajedini 2013). No metallicity gradient was found in the red giant branch star population in 28 populous LMC clusters (Grocholski *et al.* 2006) and in the outer disk of the LMC (Carrera *et al.* 2011). Piatti and Geisler (2013) also report no metallicity gradient in their analysis of an age–metallicity relationship of the LMC field star population. Interestingly, Haschke *et al.* (2012) and Deb and Singh (2014) did not detect a metallicity gradient in the OGLE-III RRab data.

Several authors, who report no gradient, argue that the errors on the mean metallicity values in distance bins are much larger than the gradient itself, thus questioning its existence. However, our study contains a much more extended area around the LMC, out to ≈ 15 kpc, and we observe a consistent decrease in median $[\text{Fe}/\text{H}]$ over that range. In addition, there is a clear evidence that the proportion of metal-rich to metal-poor RRab stars decreases with distance from the center, giving another argument for the metallicity gradient.

Our results for the inner and outer parts of the LMC are consistent with those of Wagner-Kaiser and Sarajedini (2013), who found a gradient with a slope of -0.027 ± 0.002 dex/kpc within the inner 5 kpc. On the other hand, the slope we find is steeper than the slope of -0.015 ± 0.003 dex/kpc from Feast *et al.* (2010), when taking into account the inner parts of the galaxy, but consistent within errors, if we take the total gradient value for the LMC of -0.019 ± 0.002 dex/kpc. Both studies were based on OGLE RR Lyr stars. Cioni (2009) found a decrease of iron abundance of -0.047 ± 0.003 dex/kpc out to ≈ 8 kpc, derived from the asymptotic giant branch (AGB) stars, which is steeper than found in this study. Interestingly, they noticed that the AGB gradient at $5 < r < 8$ kpc is marginally flatter than in the inner disk, which is consistent with the transition between inner disk and outer disk/halo components. We see this break with RRab stars, whose $[\text{Fe}/\text{H}]$ gradient actually flattens in that distance range.

In the case of the SMC, the metallicity gradient was found among 350 red giant branch stars in 13 fields in different positions out to $\approx 4^\circ$ from the SMC center (Carrera *et al.* 2008) and among 3037 red giants spread across approximately 37.5 deg^2 centered on this galaxy (Dobbie *et al.* 2014). Kapakos and Hatzidimitriou (2012) also found a metallicity gradient among OGLE-III RRab stars. Con-

trary, Cioni (2009) – from AGB stars, Parisi *et al.* (2009) – from the study of 16 SMC clusters, and Deb *et al.* (2015) – from OGLE-III RRab sample, report no gradient, and we support this result with our findings.

7. Summary

We used the OGLE-IV collection of fundamental mode RR Lyr stars to find a new relation between the phase parameter ϕ_{31} in the V - and I -band, in order to facilitate $[\text{Fe}/\text{H}]$ calculation for large datasets of I -band RRab light curves. The relation is non-linear and depends on metallicity, so its applicability is limited. If the metallicity-independent version of the relation is used, the final $[\text{Fe}/\text{H}]$ distribution is subject to systematic errors at the high and low ends, such that the low metallicity values are overestimated and high metallicity values are underestimated. The median of the $[\text{Fe}/\text{H}]$ distribution is not affected.

The comparison of the new photometric metallicity calculation method by Nemeč *et al.* (2013) with the widely used methods of Jurcsik and Kovacs (1996) and Smolec (2005) shows that the problem of overestimating $[\text{Fe}/\text{H}]$ at low metallicity values by the two latter methods is non negligible, when the metallicity-dependent ($\phi_{31}^I \rightarrow \phi_{31}^V$) transformation is used together with the Nemeč *et al.* (2013) method. However, when the metallicity-independent ($\phi_{31}^I \rightarrow \phi_{31}^V$) transformation is applied, the differences are smaller.

We use the method of Nemeč *et al.* (2013) to construct a photometric metallicity map of the Magellanic System from OGLE-IV RRab using the metallicity-independent ($\phi_{31}^I \rightarrow \phi_{31}^V$) relation. We find that the mean iron abundance in the LMC is -1.39 ± 0.44 dex, which is consistent with previous findings. In the case of the SMC, mean $[\text{Fe}/\text{H}]$ is -1.77 ± 0.48 dex and it is lower than values from the literature, which is explained by larger discrepancies between methods of $[\text{Fe}/\text{H}]$ calculation at low metallicities, such as those observed in the SMC.

While there appears to be no, or very mild, metallicity gradient in the SMC, we clearly see that in the LMC $[\text{Fe}/\text{H}]$ decreases with distance from the galaxy center. The decline is evident within 4 kpc from the center, then the metallicity remains constant until about 8 kpc, when it shows another slight decline out to ≈ 13 kpc. The slope of the gradient is -0.029 ± 0.002 dex/kpc in the inner 5 kpc and -0.030 ± 0.003 dex/kpc beyond 8 kpc. The total slope, for the entire LMC, is -0.019 ± 0.002 dex/kpc.

Acknowledgements. We would like to thank the anonymous Referee for remarks that greatly improved this paper. D.M.S. is supported by the Polish National Science Center (NCN) under the grant no. 2013/11/D/ST9/03445 and the Polish Ministry of Science and Higher Education under the grant “Iuventus Plus” No. 0420/IP3/2015/73. The OGLE project has received funding from the NCN grant MAESTRO 2014/14/A/ST9/00121 to AU.

REFERENCES

- Alcock, C.J., *et al.* 2000, *AJ*, **119**, 2194.
- Benkő, J.M., *et al.* 2010, *MNRAS*, **409**, 1585.
- Braga, V.F., *et al.* 2015, *ApJ*, **799**, 165.
- Carrera, R., Gallart, C., Aparicio, A., Costa, E., Méndez, R.A., and Noël, N.E.D. 2008, *AJ*, **136**, 1039.
- Carrera, R., Gallart, C., Aparicio, A., and Hardy, E. 2011, *AJ*, **142**, 61.
- Carretta, E., Bragaglia, A., Gratton, R., D'Orazi, V., and Lucatello, S. 2009, *A&A*, **508**, 695.
- Cioni, M.-R.L. 2009, *A&A*, **506**, 1137.
- Deb, S., and Singh, H.P. 2010, *MNRAS*, **402**, 691.
- Deb, S., and Singh, H.P. 2014, *MNRAS*, **438**, 2440.
- Deb, S., Singh, H.P., Kumar, S., and Shashi M. 2015, *MNRAS*, **449**, 2768.
- Dobbie, P.D., Cole, A.A., Subramaniam, A., and Keller, S. 2014, *MNRAS*, **442**, 1680.
- Feast, M.W., Abedigamba, O.P., and Whitelock, P.A. 2010, *MNRAS*, **408**, 76.
- Gonzalez, O.A., Rejkuba, M., Zoccali, M., Valent, E., Minniti, D., and Tobar, R. 2013, *A&A*, **552**, 110.
- Grocholski, A.J., Cole, A.A., Sarajedini, A., Geisler, D., and Smith, V.V. 2006, *AJ*, **132**, 1630.
- Haschke, R., Grebel, E.K., Duffau, S., and Jin, S. 2012, *AJ*, **143**, 48.
- Jeon, Y.-B., Ngeow, C.-C., and Nemeč, J.M. 2014, *IAU Symp.*, **301**, 427.
- Jurcsik, J. 1995, *Acta Astron.*, **45**, 653.
- Jurcsik, J., and Kovács, G. 1996, *A&A*, **312**, 111.
- Kapakos, E., Hatzidimitriou, D., and Soszyński, I. 2011, *MNRAS*, **415**, 1366.
- Kapakos, E., and Hatzidimitriou, D. 2012, *MNRAS*, **426**, 2063.
- Kinemuchi, K., *et al.* 2006, *AJ*, **132**, 1202.
- Kovács, G., and Zsoldos, E. 1995, *A&A*, **293**, L57.
- Nemeč, J.M., *et al.* 2013, *ApJ*, **773**, 181.
- Papadakis, I., Hatzidimitriou, D., Croke, B.F.W., and Papamastorakis, I. 2000, *AJ*, **119**, 851.
- Parisi, M.C., Grocholski, A.J., Geisler, D., Sarajedini, A., and Clariá, J.J. 2009, *AJ*, **138**, 517.
- Piatti, A.E., and Geisler, D. 2013, *AJ*, **145**, 17.
- Pietrukowicz, P., *et al.* 2012, *ApJ*, **750**, 169.
- Pietrukowicz, P., *et al.* 2015, *ApJ*, **811**, 113.
- Sandage, A. 2004, *AJ*, **128**, 858.
- Sans Fuentes, S.A., and De Ridder, J. 2014, *A&A*, **571**, 59.
- Smolec, R. 2005, *Acta Astron.*, **55**, 59.
- Soszyński, I., *et al.* 2009, *Acta Astron.*, **59**, 1.
- Soszyński, I., *et al.* 2011, *Acta Astron.*, **61**, 1.
- Soszyński, I., *et al.* 2014, *Acta Astron.*, **64**, 177.
- Soszyński, I., *et al.* 2016, *Acta Astron.*, **66**, 131.
- Szczygieł, D., Pojmański, G., and Pilecki, B. 2009, *Acta Astron.*, **59**, 137.
- Torrealba, G., *et al.* 2015, *MNRAS*, **446**, 2251.
- Udalski, A., Szymański, M.K., and Szymański, G. 2015, *Acta Astron.*, **65**, 1.
- van der Marel, R.P., and Cioni, M.-R.L. 2001, *AJ*, **122**, 1807.
- Wagner-Kaiser, R., and Sarajedini, A. 2013, *MNRAS*, **431**, 1565.
- Weinberg, M.D., and Nikolaev, S. 2001, *ApJ*, **548**, 712.
- Zinn, R., and West, M.J. 1984, *ApJS*, **55**, 45.